Proceedings of the 9th International Symposium on Fluid-Structure Interactions, Flow-Sound Interactions, Flow-Induced Vibration & Noise
July 8-11, 2018, Toronto, Ontario, Canada

FIV2018-158

NUMERICAL INVESTIGATION OF FLUID-SOLID INTERACTION IN CAVITATING FLOW

Yiwei Wang
Institute of Mechanics, Chinese Academy of Sciences
Beijing, China

Chao Yu
Institute of Mechanics, Chinese Academy of Sciences
Beijing, China

Jian Zhang
Beijing Electro-Mechanical Engineering Institute
Beijing, China y

ABSTRACT

To investigate the fluid-solid interaction in cavitating flow, a numerical method loosely coupling a flow solver based on the incompressible Navier–Stokes equations and a structure solver based on rigid-body equations is established in an open-source code OpenFOAM framework. In which, simulations of the cavitating flow are based on the large eddy simulation (LES) approach, Kunz cavitation model, and volume of fluid (VOF) method to present more information on the flow structure. Simulations of the structure motion are solving rigid-body equations with a fourth order Runge Kutta algorithm.

Then, considering the complexity of cavitation vortex interaction, vortex-induced vibration and cavitation-induced vibration in unsteady cavitating flow, flow past a circular cylinder is selected as the object. Cavitating and non-cavitating flow past a circular cylinder are simulated and compared to observe the influence of cavitation on the Karman vortex street and the drag coefficients on cylinder when Re=200, where Re is Reynold number based on the cylinder diameter D and the free-stream speed U. The structural vibration induced by vortex and cavitation in cavitating and non-cavitating flow are simulated and compared to observe the characteristics of cavitation-structure interaction. The results showed that that "synchronization" or "lock in" phenomenon occurs in both cavitating and non-cavitating flow when the value of F* nears 1. 2S and 2P vortex modes are predicted in both cavitating and non-cavitating flow. The oscillating amplitude of the cylinder in non-cavitating flow is larger than cavitating flow in synchronization range. But the synchronization range in non-cavitating flow is smaller than cavitating flow. At last, the reasons are briefly analyzed.

NOMENCLATURE

ρ_v	Density of vapor
ρ_l	Density of liquid
ρ_s	Density of the cylinder
D	Diameter of the cylinder
L	Length of the cylinder
U	Free-stream speed
P_∞	Environmental pressure
α	Liquid volume fraction
p_v	Saturated vapor pressure
$\dot{m}^+$	Evaporation rate
$\dot{m}^-$	Condensation rate
$t_\infty = D/U$	Characteristic time
u	Structural displacement
$\dot{u}$	Structural velocity
$\ddot{u}$	Structural acceleration
M	Structural mass
C	Structural damping
K	Structural stiffness
F	The outside force matrices on the cylinder
F_s	Structural natural frequency
F_l	Natural frequency of flow around cylinder
Δt	Time step
Co	Courant number
$\rho^* = \frac{\rho_s}{\rho_l}$	Solid-liquid density ratio
$F^* = \frac{F_s}{F_l}$	Ratio of the natural frequency of the structure to the flow
$\mathrm{Re} = \frac{UD}{\nu}$	Reynold number

$\sigma = \frac{P_\infty - P_v}{0.5\rho U^2}$	Cavitation number
$force_D$	Drag force on the cylinder
$force_L$	Lift force on the cylinder
$C_D = \frac{force_D}{0.5\rho U^2 DL}$	Drag force coefficients
$C_L = \frac{force_L}{0.5\rho U^2 DL}$	Lift force coefficients
$St = fD/U$	Strouhal number
$y_{\max}$	The actual oscillating amplitude
$A^* = \frac{y_{\max}}{0.5\rho U^2 DL/K}$	Dimensionless oscillating amplitude
f	The actual oscillating frequency
$f^* = \frac{f}{F_l}$	Dimensionless oscillating frequency
FW	Structural natural frequency in still-liquid
$FW^* = \frac{FW}{F_l}$	Dimensionless full wetted natural frequency
Q	Q-criterion
ν	Kinematic viscosity

INTRODUCTION

Cavitation is defined as the breakdown of a liquid medium under a low pressure [1]. Cavitating flow is a classic issue in the hydrodynamic field and has been extensively studied. In recent years, hence researchers pay attention to the the cavitating flow-induced vibrations. For example, Kaplan [2] experimentally observed that cavitating flows can excite 'flutter-like' vibrations with modest amplitudes on hydrofoils when the cavity length gets close to the hydrofoil chord length. A coupling was also observed by Katoetal [3] between the controlled pitching frequency of a hydrofoil and the cavity breakdown frequency, and it is called 'lock-in'. Ausoni *et al.* [4] observed that if the cavity or vortex shedding frequency comes near the structural natural frequencies, the structural vibration amplitudes would significantly increase and affect the cavity/vortex shedding patterns. De La Torre *et al.* [5] measured the natural frequencies a hydrofoil under different cavitation condition to investigate the added mass effect on the fluid-structure system. They found that the maximum added mass effect occurs with still water and the minimum with super cavitation. Ducoin *et al.* [6] have experimentally studied the cavitating flow around both a stationary and pitching flexible hydrofoil, and showed that cavitation can excite the wetted natural frequencies of the hydrofoil. In a numerical study, Akcabay [7] showed that the fluctuating parts of the hydrodynamic loads and deformations can get as big as their mean values under cavitating conditions, especially when the maximum cavity length comes close to the foil chord length. Wang *et al.* [8] reviewed the recently experimental tools to obtain comprehensive flow field data, and the computational tools for unsteady cavitating flow and its induced vibrations.

Those investigations mainly paid attention to the characteristics of flow structure and cavity shedding when the resonance-induced lock in occurs, rarely studied the cavitation effects on VIV in frequency domain. In comparison with the flow past a circular cylinder, their flow structure are relatively complex, which is disadvantageous for investigation of effects of cavitation on VIV. Considering the complexity of cavitation vortex interaction, vortex-induced vibration and cavitation-induced vibration in unsteady cavitating flow, a classical and widely researched flow past a circular cylinder is selected to investigate the laws of cavitation-structure interaction in this paper.

NUMERICAL METHOD

To investigate the fluid-solid interaction in cavitating flow, a numerical method loosely coupling a flow solver based on the incompressible Navier–Stokes equations and a structure solver based on rigid-body equations is established in an open-source code OpenFOAM framework.

Fluid solver

Simulations of the unsteady cavitating flow are based on the large eddy simulation (LES) approach with an one equation eddy viscosity (kEqn) subgrid scale model , a mass transport cavitation model, and volume of fluid (VOF) method to present more information on the flow structure [9-12].

In the unsteady cavitation flow, the transition between liquid and vapor is complex. In this study, the mass transfer rate is based on the Kunz model [19]:

$$\dot{m}^+ = \frac{C_v \rho_v \alpha \min\left[0, \overline{p} - p_v\right]}{(0.5\rho_l U^2) t_\infty} \quad (1)$$

$$\dot{m}^- = \frac{C_c \rho_v \alpha^2 (1-\alpha)}{t_\infty} \quad (2)$$

The empirical constants are set to $C_v = 200$ and $C_c = 100$ which are based on considerable computing experience [10-12].

Structure motion solver

Simulations of the structure motion are solving rigid-body equations with a fourth order Runge Kutta algorithm. The governing equation of the radius vibration of the rigid circular cylinder is the harmonic oscillators equation:

$$M\ddot{u} + C\dot{u} + Ku = F \quad (3)$$

where u, M, C and K are the structural displacement, mass, damping and stiffness; F is the outside force matrices on cylinder which is the force from flow in this case.

Because the effect of damping coefficient of the spring is neglectable (set as zero in present paper), the natural frequency (F_s) of the cylinder can be calculate as:

$$F_s = \frac{1}{2\pi}\sqrt{\frac{K}{M}} \quad (4)$$

Coupling system

A Loosely Coupled (LC) method as the fluid–structure interaction (FSI) model is used in this paper. The LC method is a partitioned FSI algorithm, as it couples the solutions of the two separated solid and fluid solvers and only require one fluid and one structure resolution per time step. Considering the lag

between the solid and fluid results, the time step is very small ($F_s \Delta t \le 1/500$ and Co<0.5) in present paper. However, as discussed by Causin et al. [13], these algorithms exhibit numerical instabilities for a given geometry, as soon as the density of the structure is lower than a certain threshold; for a given structure density, as soon as the length of the domain is greater than a certain threshold. Thus, the domain independence and the accuracy of FSI model with several density of the structure is verified in the paper. Moreover, considering the numerical instability for LC approaches discussed by Young et al. [14] that the force of fluid typically assumed to be zero at the first time step leads to over-estimation of the structural displacements and subsequently large artificial fluid forces in the next time step, we start the calculation of the FSI model after the flow fully developed. Thus, the force of fluid is the effect of flow at the first time step which avoid this numerical instability.

STUDY OBJECT AND PARAMETERS

Problem definition

In the present work, a circular cylinder with mass *M* and characteristic diameter *D* is mounted on a linear spring in the transverse direction as shown in figure 1. From dimensional analysis, the dimensionless control parameters are F^*, ρ^*, Re and σ. In which, the influence of parameter F^* is the most concerned. Thus, the value of F^* are 0.5 to 3.5 by changing the stiffness (*K*) of cylinder. The density ratio is 10. The Reynold number is *Re*=200 and the cavitation number is σ=1.0 .

Computational domain and grids

To simulate the flow past the freely vibrating circular cylinder, a computational domain is defined from the inlet at *X*=-20*D* to the outlet at *X*=40*D* and from -20*D* to 20*D* in the transverse direction (*Y*) as shown in Figure 1.

Depending on the end condition [15-17], the flow in the wake of a circular cylinder is a two-dimensional flow when Re=200. Thus, a grid with one layer in Z direction are used as shown in figure 2. In which, the top and bottom boundaries of the layer are set as symmetry condition.

The mesh spacing for the grid is $0.001D \times 0.008D$ in the azimuthal and radial directions near the cylinder and stretches to $0.035D \times 0.047D$ at approximately 3D downstream and then further stretches to $0.06D \times 0.047D$ at a distance of 7*D* downstream. The cells number of the gird is about 200 thousand for a layer of grid for the two-dimensional simulation.

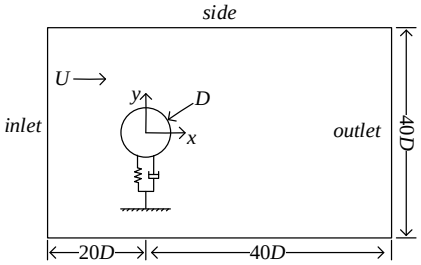

FIGURE 1: COMPUTATIONAL DOMAIN AND BOUNDARY CONDITIONS

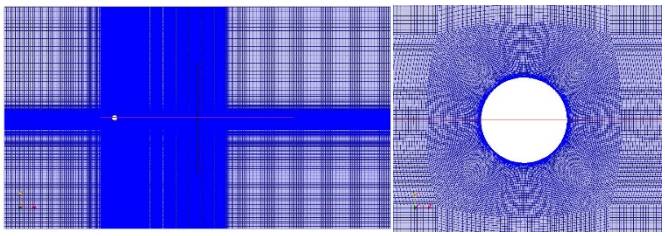

FIGURE 2: MESH FOR TOTAL (LEFT) AND LOCAL (RIGHT)

Boundary Conditions

The inlet boundary is set as velocity inlet condition with fixed velocity (*U*). The outlet boundary is set as pressure outlet condition with fixed pressure (P_∞) which is depending on cavitation number $\sigma = (p_\infty - p_{sat})/(0.5\rho U^2) = 1.0$. Two side boundaries are set as slip wall condition. The cylinder is no-slip moving wall.

Verification of grid and domain independence

To evaluate the accuracy of the simulation results, the verification of mesh independence is necessary. Insensitivity to computational grid is demonstrated using three grids for one case (Re 200 and non-cavitation). The coarse and fine grid have about 100 and 400 thousand cells respectively. The cell sizes are $\sqrt{0.5}$ and $\sqrt{2}$ times of the present grid in the azimuthal and radial directions except for the size of the first layer on the cylinder in radial direction which keeps 0.001*D*.

In the wide domain, the inlet and side boundaries are 40*D* from the cylinder, the outlet boundary is set at a distance of 60*D* downstream. The comparison of drag force coefficients (C_D) and dimensionless frequencies (*St*=*fD*/*U*) are shown in table 1.

From table 1, the deviations between the results of present grid, fine grid, coarse grid and wide domain grid are less than 1%. The time average distribution of pressure coefficients on the cylinder also presented little difference, as shown in Figure 3. Thus, the present grid and domain are fine enough to this case. Besides, from the comparison with in table 1, the numerical results keep a good agreement with the experimental results of Wen et al. [18, 19], which partly validate the accuracy of our method.

Table 1: DRAG FORCE COEFFICIENT (C_D) AND DIMENSIONLESS FREQUENCY (*St*) AT *Re*=200

	C_D	*St*
Present grid	1.38	0.199
Fine grid	1.38	0.200
Coarse grid	1.38	0.198
Wide domain	1.38	0.199
Experimental results of Wen.[18,19]	1.34±0.1	0.199

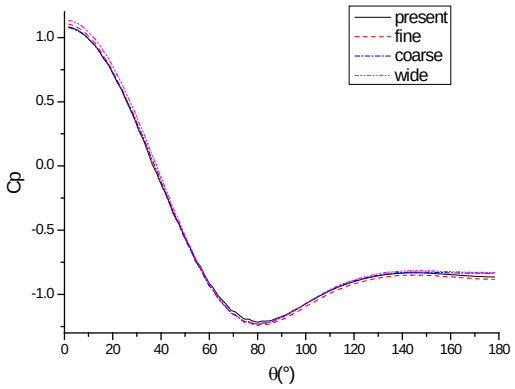

FIGURE 3: THE TIME AVERAGE DISTRIBUTION OF PRESSURE COEFFICIENT ON THE CYLINDER WITH PRESENT GRID, FINE GRID AND WIDE DOMAIN

RESULTS AND DISCUSSION

Many numerical simulations of the cylinder vibrating in cavitating and non-cavitating flow with different conditions are made. Parameters are shown in table 2.

TABLE 2: PARAMETERS OF THE FLOW

Parameters	F^*	ρ^*	Re	σ
Cavitating	0.5~3.5	10	200	1.0
Non-cavitating	0.5~3.5	10	200	-

The similarities of vibration in cavitating and non-cavitating flow

The vibration of cylinder has many similarities in cavitating and non-cavitating flow. Through numerical simulations, "synchronization" or "lock in" phenomenon [20] is captured in both cavitating and non-cavitating flow when the value of F^* nears 1. In non-cavitating flow, the vortex shedding frequency locked into the cylinder oscillating frequency (near *FW*) and a vortex formation mode "2S" (indicating 2 single vortices shed per cycle)[20] is predicted in the wake when F^*=0.9, as shown in figure 4. In cavitating flow, the cavity and vortex shedding frequencies are locked in to the cylinder oscillating frequency (near F_l) and similar "2S" mode predicted in the wake when F^*=0.9, as shown in figure 5. What's more, a vortex formation mode "2P" (meaning 2 pairs of vortices per cycle) [20] is also predicted in the wake of both cavitating and non-cavitating flow when F^*=0.7 as shown in figure 6 and 7.

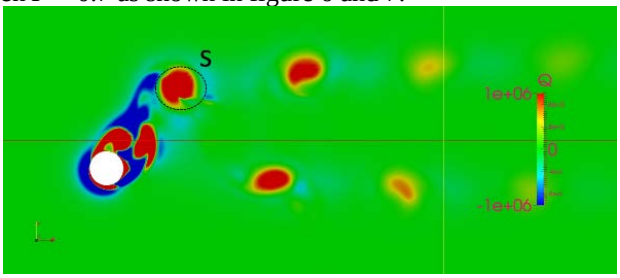

FIGURE 4: VORTEX MODE IN NON-CAVITATING FLOW WHEN F^*=0.9 (THE VORTEX STRUCTURE IS REPRESENTED BY THE Q-CRITERION [21])

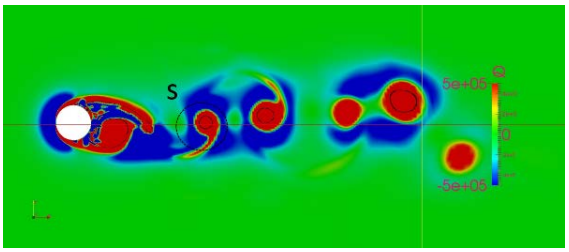

FIGURE 5: VORTEX MODE IN CAVITATING FLOW WHEN F^*=0.9 (THE BLACK LINE ARE THE ISOLINE OF α =0.9)

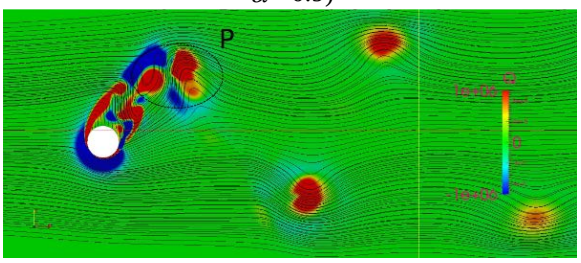

FIGURE 6: VORTEX MODE IN NON-CAVITATING FLOW WHEN F^*=0.7

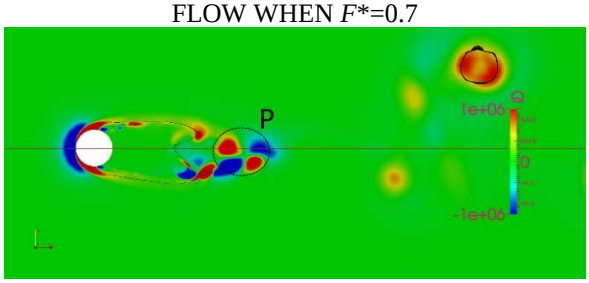

FIGURE 7: VORTEX MODE IN CAVITATING FLOW WHEN F^*=0.7

The differences of vibration in cavitating and non-cavitating flow

However, there are many differences between the vibration in cavitating and non-cavitating flow. From figure 8, the oscillating amplitude of the cylinder in non-cavitating flow is obviously larger than cavitating flow when the value of F^* nears 1. Because the pressure drop is suppressed when cavitation occurs in the low pressure zone. The fluid force in cavitation flow to be smaller than the non-cavitation flow. Although the peak force caused by cavitation collapse is larger than non-cavitating flow, the amplitude of the oscillating frequency is obviously smaller, as shown in figure 9-11.

Besides, the the oscillating amplitude of the cylinder in non-cavitating flow is smaller than cavitating flow when $1.2 < F^* \le 1.5$. That's because the different between the oscillating frequency in cavitating and non-cavitating flow. From figure 13, in non-cavitating flow, the cylinder oscillates with a frequency near the structure natural frequency in still-liquid (FW) when $0.5 \le F^* \le 1.2$. When $F^* > 1.2$, the cylinder oscillates with a frequency near the natural frequency (Fl). This is similar as the result reported by Khalak [22]. While in cavitating flow, the range rises to 1.5. Thus, when $1.2 < F^* \le 1.5$, the oscillating amplitude of the cylinder in synchronization range

in cavitating flow is larger than non-cavitating flow which is out of synchronization range.

The reason of the increases of the synchronization range in cavitating flow deserved to analyze. In one hand, the non-cavitating flow is a strong constraint comparing to cavitaing flow. Thus the vibration suppression is stronger and the oscillating amplitude drops more rapidly in non-cavitating flow when the flow out of the synchronization range. In the other hand, there are more high frequency components in the lift force in cavitating flow comparing to non-cavitating flow as shown in figure 11 and 12.

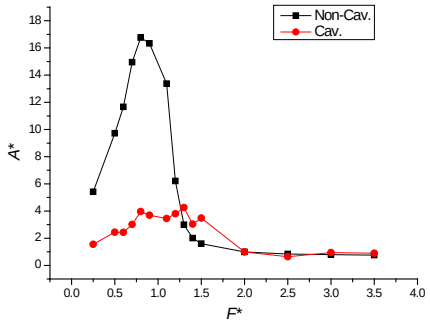

FIGURE 8: THE DIMENSIONLESS OSCILLATING AMPLITUDE *A** UNDER DIFFERENT *F**.

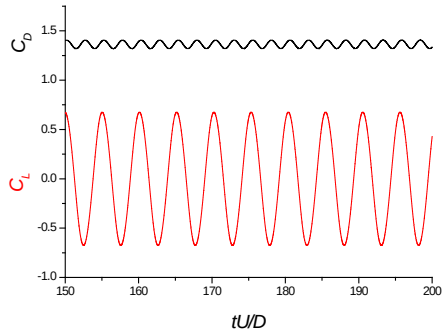

FIGURE 9: LIFT COEFFICIENT AND DRAG COEFFICIENT ON THE STILL CYLINDER IN NON-CAVITATING FLOW.

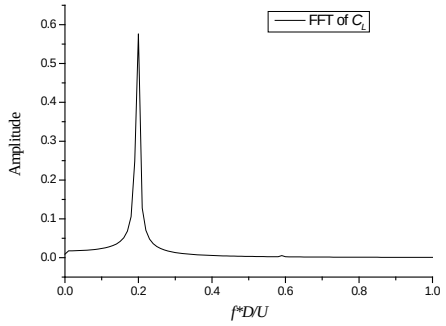

FIGURE 10: FFT FOR C_L IN NON-CAVITATING FLOW

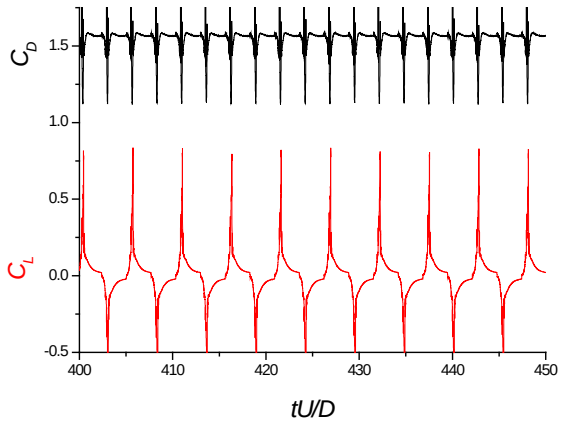

FIGURE 11: LIFT COEFFICIENT AND DRAG COEFFICIENT ON THE STILL CYLINDER IN CAVITATING FLOW.

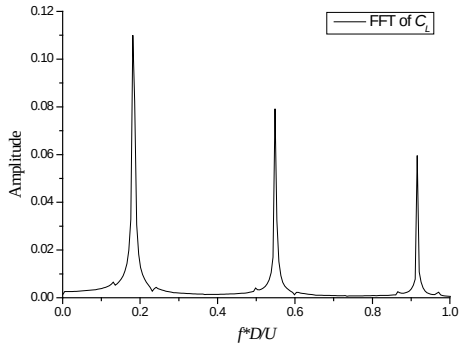

FIGURE 12: FFT FOR C_L IN CAVITATING FLOW

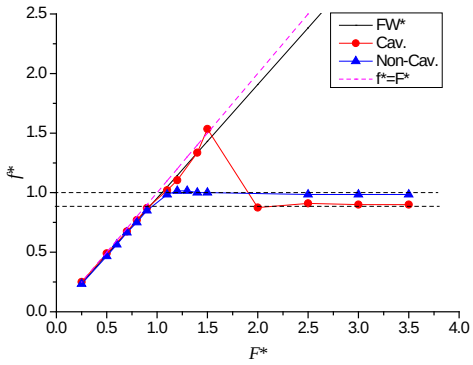

FIGURE 10: THE DIMENSIONLESS OSCILLATING FREQUENCY *f** UNDER DIFFERENT *F**.

CONCLUSIONS

A numerical method loosely coupling a flow solver based on the incompressible Navier–Stokes equations and a structure solver based on rigid-body equations is established in an open-source code OpenFOAM framework to investigate the fluid-solid interaction in cavitating flow. In which, simulations of the

cavitating flow are based on the large eddy simulation (LES) approach, Kunz cavitation model, and volume of fluid (VOF) method to present more information on the cavitaing flow structure. Simulations of the structure motion are solving rigid-body equations with a fourth order Runge Kutta algorithm.

Then, cavitating and non-cavitating flow past a circular cylinder are simulated and compared to observe the influence of cavitation on the Karman vortex street and the drag coefficients on cylinder when *Re*=200, where Re is Reynold number based on the cylinder diameter *D* and the free-stream speed U_∞. The structural vibration induced by vortex and cavitation in cavitating and non-cavitating flow are simulated and compared to observe the characteristics of cavitation-structure interaction.

The results showed that "synchronization" or "lock in" phenomenon occurs in both cavitating and non-cavitating flow when the value of F^* nears 1. The 2S and 2P vortex modes are predicted in both cavitating and non-cavitating flow. The oscillating amplitude of the cylinder in non-cavitating flow is larger than cavitating flow when $F^* \le 1.2$, but smaller than cavitating flow when $1.2 < F^* \le 1.5$. What's more, the synchronization range in cavitating flow is larger than non-cavitating flow. And the reasons are briefly analyzed.

The present method could still be improved such as adopting the closely-coupled approach, and more practical cases with high Reynolds numbers could also be investigated in the future.

ACKNOWLEDGMENTS

The authors are grateful to the national natural science foundation of China through grant numbers 11772340 & 11672315. This project was also supported by the Youth Innovation Promotion Association CAS (2015015).

REFERENCES

[1]Franc J. P., and Michel J. M., 2004. *Fundamentals of cavitation*. Kluwer Academic, Dordrecht, The Netherlands.

[2]Kamakoti, R., and Shyy, W., 2004. "Fluid-structure interaction for aeroelastic applications". *Progress in Aerospace Sciences, 40, pp. 535-558.*

[3] Kaplan, P., and Lehman, A.F., 1966. "Experimental studies of hydroelastic instabilities of cavitating hydrofoils". *Journal of Aircraft, 3, pp. 262–269.*

[4] Ausoni, P., Escaler, X., Avellan, F., Egusquiza, E., and Farhat, M., 2007. "Cavitation influence on von Kármán vortex shedding and induced hydrofoil vibrations". *ASME-Journal of Fluids Engineering, 129 (8), pp. 966–973.*

[5] De La Torre, O., Escaler, X., Egusquiza, E., and Farhat, M., 2013. "Experimental investigation of added mass effects on a hydrofoil under cavitation conditions". *Journal of Fluids & Structures, 39, pp. 173-187.*

[6] Ducoin, A., Astolfi, J.A., and Sigrist, J.F., 2012. "An experimental analysis of fluid structure interaction on a flexible hydrofoil in various flow regimes including cavitating flow". *European Journal of Mechanics – B/Fluids, 36, pp. 63–74.*

[7] Akcabay, D.T., Chae, E.J., Young, Y.L., Ducoin, A.，and Astolfi, J.A., 2014. "Cavity induced vibration of flexible hydrofoils". *Journal of Fluids & Structures, 49, pp. 463-484.*

[8] Wang, G., Wu, Q., and Huang, B., 2017. "Dynamics of cavitation–structure interaction". *Acta Mechanica Sinica, 2017, 33, pp. 685-708.*

[9]Wang, Y.W., Wu, X.C., Huang, C.G., and Wu, X.Q., 2016. "Unsteady characteristics of cloud cavitating flow near the free surface around an axisymmetric projectile". *International Journal of Multiphase Flow, 85, pp. 48-56.*

[10]Yu X.X., Huang C.G., Du T.Z., Liao L.J., Wu X.C., Zheng Z., and Wang Y.W., 2014. "Study on characteristics of cloud cavity around axisymmetric projectile by large eddy simulation". *ASME-Journal of Fluids Engineering, 136, 051303.*

[11]Yu, C., Wang, Y.W., Huang, C.G., Du, T.Z., Xu, C., and Huang, J., 2017. "Experimental and numerical investigation on cloud cavitating flow around an axisymmetric projectile near the wall with emphasis on the analysis of local cavity shedding". *Ocean Engineering, 140, pp. 377-387.*

[12] Yu, C., Wang, Y.W., Huang, C.G., Wu, X.C., and Du, T.Z., 2017. "Large Eddy Simulation of Unsteady Cavitating Flow Around a Highly Skewed Propeller in Nonuniform Wake". *ASME-Journal of Fluids Engineering, 139, 041302.*

[13]Causin, P., Gerbeau, J.F., and Nobile, F., 2005. "Added-mass effect in the design of partitioned algorithms for fluidstructure problems". *Computer methods in applied mechanics and engineering, 194, pp. 4506-4527.*

[14]Young, Y. L., Chae, E. J., and Akcabay, D. T., 2012. "Hybrid algorithm for modeling of fluid-structure interaction in incompressible viscous flows". *Acta Mechanica Sinica. 28, pp. 1030-1041.*

[15]Miller, G.D., and Williamson, C.H.K., 1994. "Control of three-dimensional phase dynamics in a cylinder wake". *Experiments in Fluids 18, pp. 26–35.*

[16]Williamson, C.H.K., and Roshko, A., 1988. "Vortex formation in the wake of an oscillating cylinder". *Journal of Fluids & Structures, 2, pp. 355–381*

[17]Williamson, C.H.K., 1989. "Oblique and parallel modes of vortex shedding in the wake of a circular cylinder at low Reynolds numbers". *Journal of Fluid Mechanics 206, pp. 579–627.*

[18] Wen C.Y., and Lin C.Y., 2001. "Two-dimensional vortex shedding of a circular cylinder". *Physics of Fluids, 13, pp. 557-560.*

[19]Wen, C.Y, Yeh, C.L., Wang, M.J., and Lin, C.Y., 2014. "On the drag of two-dimensional flow about a circular cylinder". *Physics of Fluids, 16, pp. 3828-3831.*

[20] Khalak, A., and Williamson, C.H.K., 1999. "Motions, forces and mode transitions in vortex-induced vibrations at low mass-damping". *Journal of Fluids & Structures, 13, pp. 813-851.*

[21] Sahner, J., Weinkauf, T., and Hege, H.C., 2005. "Galilean Invariant Extraction and Iconic Representation of Vortex Core Lines." *Proc. EUROGRAPHICS-IEEE VGTC Symposium on Visualization, Leeds, United Kindom.*